CFD Analysis of the Aerodynamic Effects of a Gurney Flap on a Small-Scale Horizontal Axis Wind Turbine with a Low Reynolds Number

By Onur Mert Aksoy

SEMS MSc Research Dissertation, 2019-2020

Supervisor: Dr Eldad Avital

Declaration:

SCHOOL OF ENGINEERING AND MATERIALS SCIENCE

ENGINEERING / MATERIALS
MSc Final Report
2020

DECLARATION

This report entitled:

CFD Analysis of the Aerodynamic Effects of a Gurney Flap on a Small-Scale Horizontal Axis Wind Turbine with a Low Reynolds Number

Was composed by me and is based on my own work. Where the work of the others has been used, it is fully acknowledged in the text and in captions to table illustrations. This report has not been submitted for any other qualification.

Name: Onur Mert Aksoy

Signed: 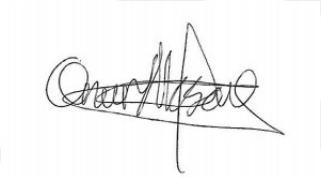

Date: 09/09/2020

Acknowledgements

I would first like to thank my thesis supervisor Dr E.Avital who has provided continuous supervision of my work and steered me in the right direction whenever he thought I needed it. He made sure that the current lockdown situation did not affect the quality of the work that I produce by replying to emails and arranging meetings almost instantly when it was needed. He also gave me permission to use the high spec computer system available by the Queen Mary University of London which was critical for me to be able to complete my project. Overall the supervisor role taken by Dr E.Avital was phenomenal.

I would also like to thank family for the support that they have always given me for all my aspirations. They have done their best to transform our current living arrangement for me to be able to work on my thesis and have done their best to reduce the stresses caused by the many complications of the COVID pandemic.

Lastly, I would also like to thank my sincere friends who have been very motivational and were a critical part of reducing the stresses caused by the COVID pandemic in my life.

Abstract:

CFD analysis was used to investigate and optimize the effect of a Gurney flap on a low Reynolds aerofoil, the Eppler E387, to improve the performance of small-scale wind turbines. 2D Unsteady RANS simulations were employed with ANSYS to investigate the affect of the Gurney flap. Validation process was successfully taken place on the E387 aerofoil without a Gurney Flap before investing the effect of Gurney Flaps with heights, in percentage of the aerofoil chord length, 1c%, 1.5c%, 2c% and 3c%. This lead to the discovery the lift was enhanced with increasing Gurney flap height due to the distinctive counter rotating vortices formed by the Gurney flap. However, at high AoA the drag penalties become more severe which leads to an earlier stall. Once flow fields of each Gurney flap height were analysed, the optimum CL/CD ratios of each Gurney flap setting was used to calculate the optimum tip speed ratio and the coefficient of power with single rotor calculations assuming linear aerodynamics.

Table of Content

List of Figures:

1. Introduction:

The development of renewable energy is a key factor to reduce our dependency on fossil fuels. The traditional use of finite fossil fuels is not sustainable whereas renewable energy has the advantage of being a non-polluting and an infinite source of energy. Wind energy plays a big role in this sector (Dilimulati, Stathopoulos and Paraschivoiu, 2018), especially large-scale wind turbines (LSWT's) in rural terrains and wind farms which are presently very efficient and dominated by horizontal axis wind turbines (HAWT). However, developing efficient small-scale WT's for an urban environment is underdeveloped and is a new area of application that can reduce our dependency on fossil fuels.

HAWT are wind turbines with their rotor shaft and electrical generator parallel to the direction of the wind. Unlike large scale HAWT's, small scale HAWT's are placed where the power is required and where the aerodynamic qualities of the environment may not be ideal.

The chord-based Reynolds number at different blade sections of a small-scale wind turbine (SSWT) blade (Shen et al., 2016) is exceptionally lower due to the smaller sizes and dimensions combined with low wind conditions in comparison to large scale wind turbines (LSWT). Airfoils that operate below Re=500 000 (Singh and Ahmed, 2013), where the flow across the upper surface of the airfoil is mostly laminar, suffer from laminar separation bubble and laminar flow separation. This can result in the loss of aerodynamic performance, like decrease in lift and increase in drag.

A Gurney Flap (GF) is a passive augmentation device (Aramendia et al., 2019), a device that does not require external energy consumption, invented by Dan Gurney in 1960. It is a small tab placed normal to the airfoil surface close to the trailing edge either in the upper or lower side that enhances the lift of the airfoil.

In this thesis the Gurney flap technology will be investigated with the Eppler 387 airfoil to optimize its performance at low Reynolds numbers with the use of computational fluid dynamic analysis and blade element momentum theory methods.

1.1. Aims and objectives:

Project Aims:

- To investigate and optimize the aerodynamic effect of a Gurney Flap on Eppler E387 low Reynolds number profile airfoil and its effect on a small-scale Horizontal Axis Wind Turbine (HAWT) performance.

Project objectives:

- Literature review on small scale HAWT's and Gurney Flaps- Research of the existing technology and background to justify the feasibility of the project and to gain knowledge.
- Study of methodology- To study how to how to use CFD and CAD software to complete successful 2D simulations.
- 2D CFD analysis of E387 profile airfoil without Gurney Flaps.
- Validation of 2D CFD results- Compare results to existing data of the E387 profile airfoil without gurney flaps
- 2D CFD analysis of E387 profile airfoil with different selected Gurney Flap heights
- Determine the optimized Gurney Flap configuration- Comparison of all simulation results to discover which Gurney Flap configuration provides the highest Cl/Cd values.
- Optimum coefficient of power calculation for a single rotor with optimum values of lift and drag coefficients obtained from each gurney flap configuration.

2. Literature Review:

2.1. Small Scale Wind Turbines and Laminar Separation Bubble Phenomena

The raising level of greenhouse gas emissions (Ledo, Kosasih and Cooper, 2011), global warming and increasing prices of fossil fuels have brought the attention into low-cost small-scale wind turbines. SSWT's can be integrated on domestic house roof tops, farms, and remote communities (Ozgener and Ozgener, 2007) where the wind conditions are not ideal to produce wind power (Singh and Ahmed, 2013) whereas for larger horizontal axis wind turbines are located at areas with optimum wind conditions.

SSWT's experience low Reynolds flow on their turbines blade due to low wind speeds conditions and small rotor sizes. At low Reynolds numbers the SSWT's can suffer from laminar separation bubble (LSB). For Reynolds Flow at 500,000 (Winslow *et al*., 2018), LSB can occur when the flow is subjected to a large adverse pressure gradient (APG). This flow separates as a shear layer due to the low kinetic energy of the laminar boundary layer. LSB is then formed as the shear layer gains momentum from the free stream and reattaches as a turbulent boundary layer. For Reynolds flow below 500,000(Singh and Ahmed), aerofoils are at susceptible to laminar flow separation which is when the separated boundary layer does not reattach to the surface downstream which could lead to stall.

The formation of LSB degrades the overall aerodynamic performance of an aerofoil (Ozgener and Ozgener), including the turbines start up and power coefficient. This is because of the increased boundary layer thickness caused by the separation bubble which results in an increase in pressure drag and lower aerodynamic lift (Mayer *et al*., 2001).

Due to these affects caused by LSB researchers have been investigating how an augmentation device could supress or counter the influence of LSB to improve the performance of SSWT's that operate in low Reynolds flow conditions.

2.2. Gurney Flaps

A potential device to improve the flow properties of low Reynolds flow over SSWT's blades is a Gurney Flap (GF). GF's were first used in 1960 by a US driver Dan Gurney (Aramendia *et al*., 2019) who places a small tab perpendicular to the trailing edge rear spoilers of F1 vehicles, on the pressure side, resulting in increased aerodynamic performance. This would consist of higher downforce which would be beneficial for traction of the F1 vehicle. This discovery then leads to

the systematic experimental campaign on a Newman airfoil by Liebeck (1978) which confirmed that GF's could improve the lift force on aerofoils.

As shown in Figure 1, Leibeck assumed that the flow field around the airfoil experiences changes consisting of the formation of a stagnation zone upstream of the GF and two counter rotating vortices downstream of the GF.

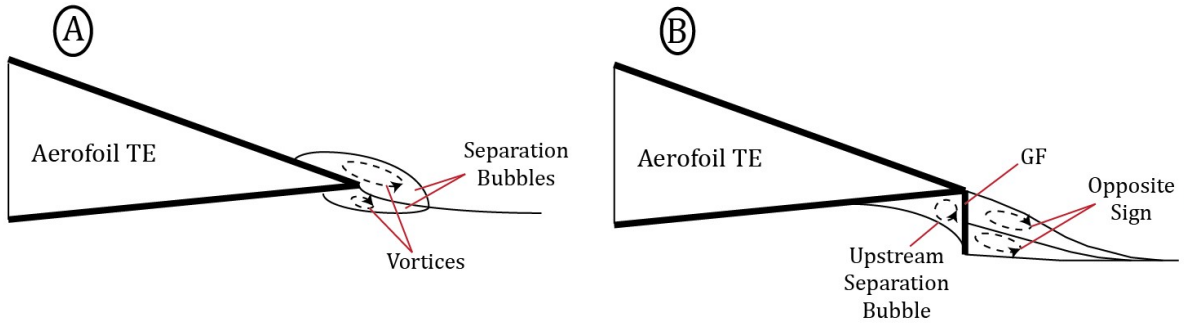

Figure 1, Flow field around aerofoil with no GF, (B) Flow field around an aerofoil with a Gurney Flap. Diagram adapted from Bianchini, et al., (2019).

Liebeck (1978) found that the GF height should be kept between 1% and 2% chord length of the airfoil to maximize the aerodynamic benefits which otherwise could be invalidated by the increase in drag. With moderate GF height, the small separation region on the suction side of the aerofoil (Jang *et al.,* 1998) contribute to counteracting the drag physically caused by the existence of the GF.

Bianchini, *et al.,* (2019) states that further studies on GF's confirmed the existence of these vortices formed by the GF and that it was responsible for an increase of suction on the aerofoil upper surface and pressure on its lower surface resulting in considerably large increase in lift coefficient. The low-pressure region (Jang *et al.,* 1998) behind the GF causes a downward momentum of fluid in the region above the trailing edge. These characteristics are also highlighted in recent research like numerical study by Yan *et al*., (2019) where it is also shown that stall was experienced at a lower angle of attack in comparison to an aerofoil without GF.

Yan *et al*., (2019) also investigated the affects of the mounting angle of the GF at 45° 60° and 90° which showed that the flap with mounting angle 90° provided better performance for lift enhancement in comparison to the other two mounting angles near the stall conditions by approximately 5%. In terms of CD it is found that the CD is almost unchanged at AoA ranging from 0° to 13° with the three GF mounting angles. Otherwise, at higher AoA ranging from 14° to 20°, the drag penalty by the GF increases with higher mounting angles.

Hao and Gao, (2019) also investigated the affect of the Gurney Flap width of the S809 aerofoil. Three GF widths of0.2%, 0.6% and 1.0% of the chord was used with a GF height of 2% chord. The

results displayed that the GF generates higher lift coefficients as the flap width decreases. However, it was concluded that the change in GF width had an insignificant affect.

In terms of the performance of a GF, current research dictates that the GF height is the main factor that determines the performance of the GF and that the GF mounting angle can have significant affects on CD only at high AoA's hence, for optimum lift enhancement the GF angle should be kept at 90°.

2.3. CFD Modelling

Numerical studies can be performed with the use of Computational Fluid Dynamic (CFD) analysis software's like ANSYS Fluent. ANSYS fluent is a simulation software used to predict fluid flow, heat and mass transfer and other related phenomena. Many researchers implement the use of ANSYS Fluent into their research as it is a cost affective way of developing research.

For accurate CFD modelling, the key factors affecting this includes the domain size, mesh structure boundary conditions and the turbulence model.

In terms of modelling low Reynolds flow of an aerofoil in ANSYS, Yan *et al*., (2019), Sreejith and Sathyabhama, (2018) and He *et al.,* (2017) use a C shape domain. To achieve a fully developed flow Yan *et al*., sets the domain size to have the aerofoil section 10 times the chord length, referred as 10c, away from the inlet and 15c away from the outlet whereas Sreejith and Sathyabhama and He *et al.,* used larger domain sizes.

Keeping the domain size as small as possible is beneficial to decrease the computation cost and time of the simulation hence achieving a fully developed flow with a smaller domain is ideal. The journals mentioned above use structured grids rather than unstructured to avoid divergence of rough grids and have employed a H type mesh. For boundary conditions a velocity inlet and a pressure outlet are employed.

In relation to Reynolds- averaged Navier-Stokes (RANS) turbulence modelling, ANSYS (2009) states that turbulent flows are defined by fluctuating velocity fields. These fluctuations mix transported quantities like momentum, energy, and species concentration, which cause the transported quantities to fluctuate. Direct simulation of these fluctuations is too computationally expensive since these fluctuations can be of small scale and high frequency. Alternatively, the instantaneous governing equations can be time-averaged to remove the resolution of small scales, resulting in a modified set of equations that are more cost effective to solve. However, the modified equations contain additional unknown variables where turbulence models are required to determine them in terms of know quantities.

To select the most suitable model for this scenario, Aftab *et al.,* (2016) compares the advantages and disadvantage of four turbulence models that can be used to model the transition of laminar to turbulent flow during LSB at Reynolds 120,000. The evaluated turbulence models consisted of one equation Spallart Allmars (S-A), two equation SST K- ω, three equation intermittency (γ) SST, k-kl- ω and finally, the four-equation transition γ-Reθ SST model. It was shown that the four-equation transition γ-Reθ SST model provided the most reliable results in comparison to the other models as it was able to capture flow physics accurately at low and high AoA's.

Xiang (2017) has also performed a similar investigation and also came to the conclusion that the four equation Transition SST model focuses more on the boundary layer behaviour with greater consideration of turbulent intermittency and boundary layer momentum thickness which produced predictions on the aerofoil performance near the stalling angle with higher accuracy in comparison to other models available. Hence, Xiang and Aftab *et al.,* chose to use the four equation Transition SST model. However, it will not be overlooked that Yan *et al*., (2019) has achieved successful results with the 2-equation k-omega SST model therefore these two models will be of interest for this project.

3. Methodology:

To be able to model the low Reynolds flow over the Eppler 387 aerofoil. A simulation of the aerofoil without GF must be performed and compared against experimental data to validate the performance of the ANSYS simulation.

The experimental data used to validate results are from Xiang (2017) PhD thesis where a subsonic wind tunnel test in Queen Mary University of London on the aerofoil E387 was performed at Reynolds numbers of 100,000 and 200,000. In this section, the methods used to attain results will be discussed in detail.

3.1. Numerical Solution

In this study, 2D unsteady pressure-based method was used to compute the incompressible flow over the Eppler 387 aerofoil. This pressure-based solver applies an algorithm which classifies as the projection method. In this method (ANSYS, 2009), the constraint of mass conservation (continuity) of the velocity field is achieved by solving pressure correction equations. The pressure equation is derived from continuity and the momentum equations so that the velocity field, corrected by the pressure, satisfies the continuity.

Considering that the governing equations are nonlinear and coupled to one another, the solution reaches convergence by iterations where the governing equations are solved repeatedly (ANSYS). A main advantage of using an unsteady (coupled) solver in comparison to a segregated solver is

that the rate of solution is significantly improves. However, the memory requirements increase by 1.5- 2 times.

The assumption of the Reynolds decomposition introduces a set of unknown functions of the velocity fluctuations called the Reynolds stresses. These require a turbulence model to produce closed system of solvable equations. Due to research performed by Xiang (2016), Aftab *et al.,* (2017) and Yan *et al*., (2019), the four equation Transition SST model and the two equation k-omega SST model will be used to investigate the effect of a GF on the E387 aerofoil.

The two-equation k-omega SST model Aftab *et al.,* (2017) is a mixture of the Wilcox k-omega and the standard k-ε model. The benefit of the near wall treatment linked with the Wilcox model is utilised by blending the two equations. Hence, the sub- viscous layer effects in the inner layer is captured by the standard k-ε as well as the outer layer effects captured by the k-omega model.

The four equation Transition SST model is based on $k-\omega$ SSt model, with 2 additional equations for intermittency (γ) and for transitional Reynolds number ($Re_{\theta t}$) to model the laminar-turbulent transition process (Menter *et al.,* 2006). Downstream of the transition point in the boundary layer the intermittency term is used to activate the production term of the turbulent kinetic energy (TKE) and the transition Reynolds number term captures the non-local effect of the turbulence intensity.

All simulations were performed with a pressure-velocity coupling scheme of 'Coupled' with spatial discretization and transient formulation in the second order for the solution to be solved at a higher accuracy by the boundary layers.

Reference values in ANSYS are used to calculate coefficients like CL and CD hence these settings are very influential. The chord of the aerofoil model in Xiang (2016) experimental set up is 0.2286 metres with a span of 0.76 metres. The ANSYS geometry of the model has the same chord whereas the span is not set since the simulation is in 2D but in the reference values, ANSYS automatically sets the depth of the set up at 1 metre. This would provide false results as the depth should be set at the aerofoil span used in the experimental data hence the depth was changed to 0.76 metre along with the reference area which would be represented by the planform area.

A time step size of 0.001 seconds, 15 max iterations and 1000-time steps allowed the solution to converge by 1 second flow time for AoA's 0° to 12°. This numerical set up was used for all the simulations.

3.2. Computational Domain and Boundary Conditions

With consideration of mentioned studies performed in the literature review section about numerical investigation of low Reynolds flow over an aerofoil, a C shape domain was used to model this analysis. Initially the distance of domain walls was set to be set at 20 times the chord length, referred as 20c, from the aerofoil in all directions. The rear vertical wall is set as a pressure outlet and the remaining walls are set as a velocity inlet. The aerofoil was set as a wall will no-slip condition.

This boundary setting allows the model to be simulated at any required angle of attack (AoA) without having to re-mesh the model for each AoA by adjusting the X and Y flow component directions from the inlet. As a result, the physical time taken to set up simulations are reduced drastically.

The domain size was also reduced in small increments to test if the flow would be affected by the boundary locations by checking if there is a change in the Cl, CD, and physical contour diagrams to achieve an optimum domain size. Hence, the following domain size shown in Figure 2 was obtained where no change in calculated coefficients or reverse flow was observed. This reduced the computational time and cost of each simulations as less elements are now required to successfully mesh the model with a smaller domain.

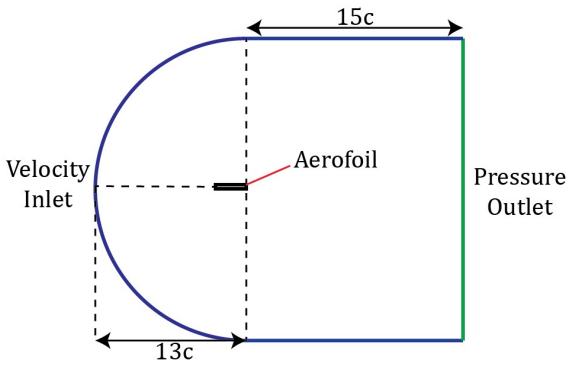

Figure 2, Final Domain Dimensions

The velocity magnitude was set as 6.39m/s and 12.79 m/s to set a chord-based Reynolds flow of 100,000 and 200,000 to validate the results against the wind tunnel test in Xiang (2017) PhD thesis. The corresponding turbulence intensities were set as 0.61% and 0.46% which was measured at the centreline empty section of the wind tunnel test.

3.3. Mesh Structure and Refinement

3.3.1. Clean Aerofoil

Design modeller in ANSYS workbench is employed to mesh the E387 aerofoil in a H shape. The H shape partitions were modified by the leading edge and set at an angle perpendicular to the surface to achieve a more even mesh near the surface of the aerofoil as shown in Figures 4 to 6.

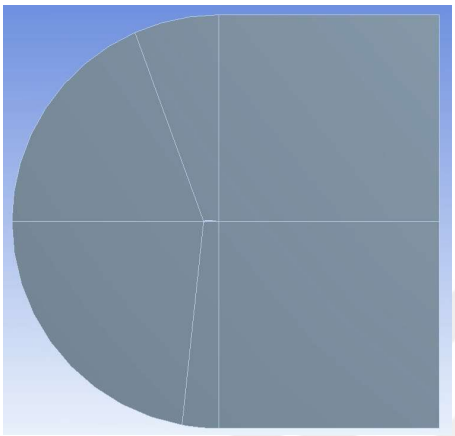

Figure 3, Partitions on the Domain

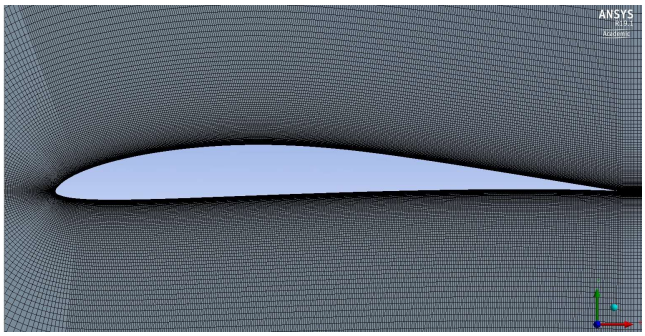

Figure 4, Overview Mesh of the E387 Aerofoil

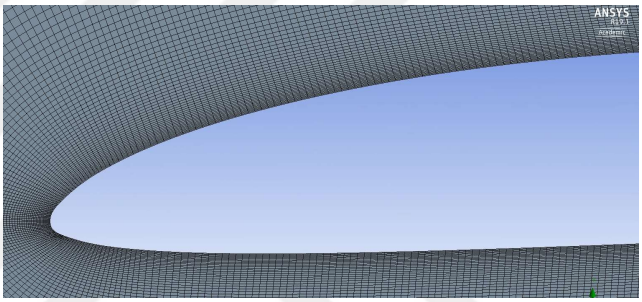

Figure 5, Zoomed Mesh View of E387 Aerofoil

The vertical distances from the aerofoil are meshed into 150 divisions with a 1.05 growth rate ensuring a Y-plus value less than 1. This allows the solution to solve the viscous sub layer and models the transition of laminar to turbulence accurately as a near wall treatment model is automatically employed with both turbulence models used.

To be able to validate numerical results against the experimental data, a mesh refinement process must be performed where a coarse mesh is refined up till a point where there is no change in results. This ensures that an over-defined mesh is not used for further simulations, saving computational cost and time.

Three meshes were used to refine the mesh made up of 54000, 126000 and 243200 elements labelled as Mesh 1, 2 and 3 with the four-equation transition SST model. The mesh was mainly refined near the aerofoil region while maintaining a y-plus value less than 1 until there was no significant change in CL and CD values. Skewness quality was monitored when creating the meshes to ensure the achievement of a high-quality mesh. Skewness is the difference between the shape of the cell and the shape of an equilateral cell of equivalent volume and an average value less than 0.33 must be obtained for high quality.

The average skewness of all the meshes used were approximately 0.005. The mesh refinement was performed with Reynolds 100,000 at AoA 0° with the Transition SST model.

Table 1, Mesh Refinement of E387 Aerofoil with no GF

Mesh Refinement			
Mesh No	Number of Elements	CL	CD
1	54000	0.37144	0.01485
2	126000	0.37073	0.01502
3	243200	0.37000	0.01501

As shown in Table 1 The CL was more sensitive to the mesh in comparison to the CD where the maximum change in CL was 0.39% whereas for the CD it was 1.14%. It is shown that the difference between mesh 1 and 2 results were not significant, but due to the availability of a high spec computer and the fact that the least difference was observed between mesh 2 and mesh 3, mesh 2 was chosen as the optimum mesh to use to model all 100,000 and 200,000 Reynolds flows with the transition SST and k-omega SST model for highest accuracy.

3.3.2. Aerofoil with Gurney Flap

Since more accuracy was achieved at Reynolds 200,000 with the Transition SST model, in comparison to the 100,000 Reynolds flow, as shown in the results section, this 200,000 Reynolds condition and Transition SST turbulence model was used to further investigate the affects of a Gurney flap (GF). However, the k-omega SST model is considered and tested with GF to investigate the flow characteristic difference between the two turbulence models and to decide which model data to use to calculate optimum coefficient of power values for a single rotor.

Mesh 2 settings were applied to model the aerofoil with the GF however the bottom surface and the wake required further refinement to achieve a low boundary layer height around the GF so that a wall y-plus of less than 1 is achieved. To maintain a high-quality mesh, so that there is no major cell size difference across the mesh, the top of the aerofoil is also refined the same way as the bottom surface. The total number of divisions on the top and bottom surface of the aerofoil is 200 which captures the characteristics of the LSB well. A bias is set to gradually decrease the cells size near the leading and trailing edge as shown in Figures 6-8.

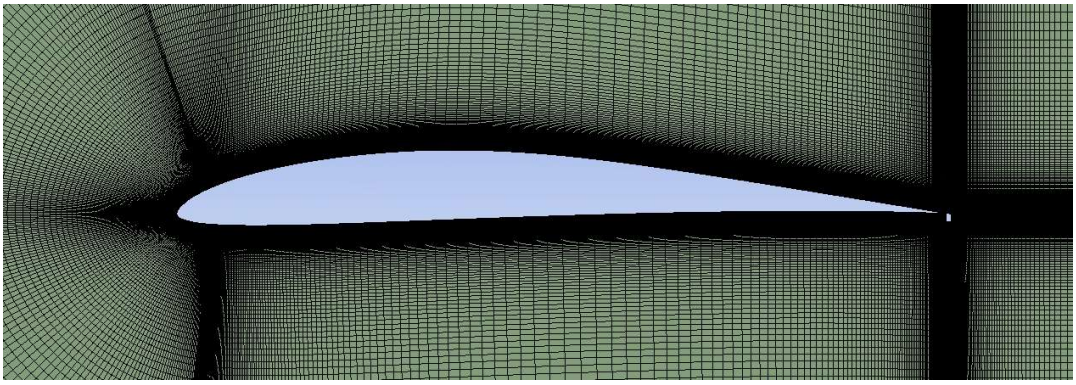

Figure 6, Mesh A of E387 Aerofoil with 1c% GF

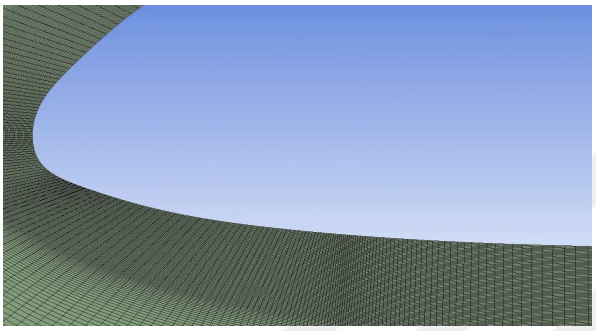

Figure 7,Bottom Leading Edge Zoomed View of Mesh A

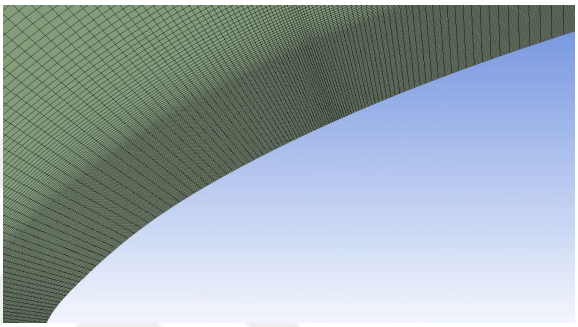

Figure 8,Upper Leading Edge Zoomed View of Mesh A

The trailing edge cell size is particularly important to create a small boundary layer height on the inside of the GF. Overall, the first cell height around the aerofoil is 3.582e-5 metres and 5.242e-5 metres around the gurney flap. Figure 9 and Figure 10 shows the physical mesh structure around the aerofoil GF with Height 1c% and 3c% (Figures 9 and 10 are not at the same scale).

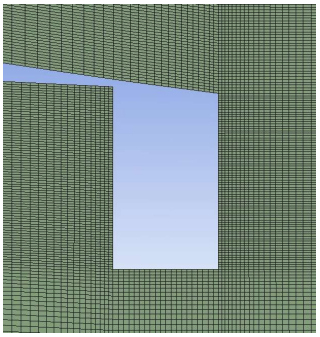

Figure 9, Mesh of Gurney Flap 1c%

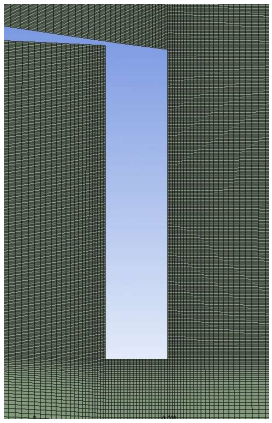

Figure 10, Mesh of Gurney Flap 3c%

The number of elements was increased from 129,000 to 200,100 elements for the 1c% GF in comparison to the aerofoil without GF. An average wall y-plus value of 0.701 is kept constant.

To check the validity of this mesh, the mesh structure was further refined around the aerofoil one more time with the mesh settings, CL and CD results shown in Table 2 below. For this mesh refinement process the transition SST model is employed.

Table 2, Mesh Refinement of E387 Aerofoil with 1c% GF

Mesh	Number of Elements	CL	CD
A	200100	0.4969	0.01025
B	405438	0.4962	0.01026

As shown in Table 2, the CL has decreased by 0.14% and CD increased by 0.1% from Mesh A to Mesh B. This change is not considered significant enough to hinder results hence, Mesh A was chosen as the most ideal mesh to perform the remaining simulations with the lowest computational cost and time.

Four GF heights were chosen in percentage of the aerofoil chord length with gurney flap thickness of 0.6c%. Only the divisions across the height of the gurney flap was increased with increasing GF size otherwise the same mesh structure mentioned was applied for all GF heights. The GF heights include 1c%, 1.5c%, 2c% and 3c%. The increase in GF height increased the number of elements for each setting due to refining the boundary layer of the gurney flap for a y-plu value less than one. The corresponding number of elements for GF 1c%, 1.5c%, 2c% and 3c% are 200100, 224410, 263250 and 323100 elements.

Running simulations with the number of elements presented on an average computer set up can be very time consuming, especially since each simulation must be repeated at multiple AoA's. Due to the availability of a high spec computer system by Queen Mary University of London and the permission of Dr Avital, a high performance set up was used to complete the following simulations.

The simulations were run from an AoA from 0° to 8° in intervals of 2° with the addition of AoA's 9°, 10° and 12°. 14° angle of attack was not run for the simulation of the aerofoil with GF to reduce workload and because only the values before stall, to calculate the lift curve slope, are required to calculate the optimum coefficient of power of a single rotor which will determine the optimum gurney flap height for a generic rotor. This is further discussed in the following section.

3.4. Calculating Optimum Coefficient for a Single Rotor

Optimum coefficient of power for a single rotor can be calculated when BEM method is coupled with an optimization algorithm with appropriate constraints. Assuming high tip speed ratio and linear aerodynamics the following equations from appendix B (Avital, 2020) and with a_opt=1/3 (Hansen, 2008).

To calculate the optimum coefficient of power (CP), the optimum tip speed ratio (TSR_{opt}) must be calculated. Where TSR is the ratio of the tangential speed of tip of the blade and the actual speed of the wind. σ is the ratio of total rotor planform area to total swept area called the solidity. CL_{opt} is chosen to be the CL at the AoA where the CL/CD ratio is the highest before stall. Hence the TSR_{opt} is calculated with the following equation below derived in appendix B (Avital, 2020).

$$\mathrm{TSR}_{opt} = \sqrt{\frac{8}{9\sigma CL_{opt}}}$$

After finding the TSR_{opt} the relative flow angle $\emptyset_T$ and the pitch angle of the blade θ_T at the tip of the blade are calculated (in radians) with the following equations where is the lift curve slope.

$$\emptyset_T = \frac{2}{3\mathrm{TSR}_{opt}}$$

$$\theta_T = \frac{2}{3\mathrm{TSR}_{opt}} \times \left(1 - \frac{8}{3\mathrm{TSR}_{opt} CL_{\alpha} \sigma}\right)$$

The values obtained now are used to calculate CP in the equation below where CD_0 is the CD at optimal CL.

$$CP_{opt} = \frac{TSR_{opt}^3 \sigma CL_{\alpha} \emptyset_T (\emptyset_T - \theta_T)}{2} - \frac{\sigma CD_0 TSR_{opt}^3}{4}$$

An example Calculation is shown below for E387 aerofoil without GF at Reynolds 200,000. In this set up, the CL_{opt}=1.00 and CD_0=0.0161. These values are taken from the highest CL/CD ratio which is at an AoA of 6°. σ is chosen to be 0.07 and the CL_{α}=6 calculated in radians.

Hence TSR_{opt} is,

$$\mathrm{TSR}_{opt} = \sqrt{\frac{8}{9\sigma CL_{opt}}} = \sqrt{\frac{8}{9 \times 0.07 \times 6}} = 3.56$$

Then flow angle and pitch angle are,

$$\emptyset_T = \frac{2}{3\mathrm{TSR}_{opt}} = \frac{2}{3 \times 3.56} = 0.187\ rads$$

$$\theta_T = \frac{2}{3\mathrm{TSR}_{opt}} \times \left(1 - \frac{8}{33.56 CL_\alpha \sigma}\right) = \frac{2}{3 \times 3.56} \times \left(1 - \frac{8}{3 \times 3.56 \times 6 \times 0.07}\right) = -1.46\ rads$$

And finally, CP is obtained by

$$CP_{opt} = \frac{TSR_{opt}^3 \sigma CL_\alpha \emptyset_T (\emptyset_T - \theta_T)}{2} - \frac{\sigma CD_0 TSR_{opt}^3}{4}$$
$$= \frac{3.56 \times 0.07 \times 6 \times 0.187(0.197 + 1.46)}{2} - \frac{0.07 \times 0.0161 \times 6^3}{4} = 0.451$$

4. Results and Discussions:

This section represents the summary of results obtained that will be discussed and analysed in detail.

4.1. Validation of Results

To be able to validate the simulations of the E387 aerofoil with a GF, simulations without the GF must be performed and compared to existing experimental data first. All RANS simulations have converged by 1e-5 with a total flow time of 1 second. Figures 11-14 shows the CL and CD results with the Transitions SST, k-omega SST model and the experimental data obtained from the wind tunnel test in Xiang's (2017) thesis.

For Reynolds flow of 100000, it can be seen in Figure 11 that the CL values of the transition SST model agrees well with the experimental data where it is slightly overestimated from AoA 2° to 8° with maximum deviation of 5%. The k-omega SST model also follows the same trend but at AoA 6° CL is underestimated by 4.33% and the corresponding CD is overestimated by 43.8% as shown in Figure 12.

Both models then underestimates the CL apart from the transition SST model at AoA 14° but it is visible that the transition SST data correlates better than the k-omega SST model as the largest corresponding difference in results is 7% and 17%.

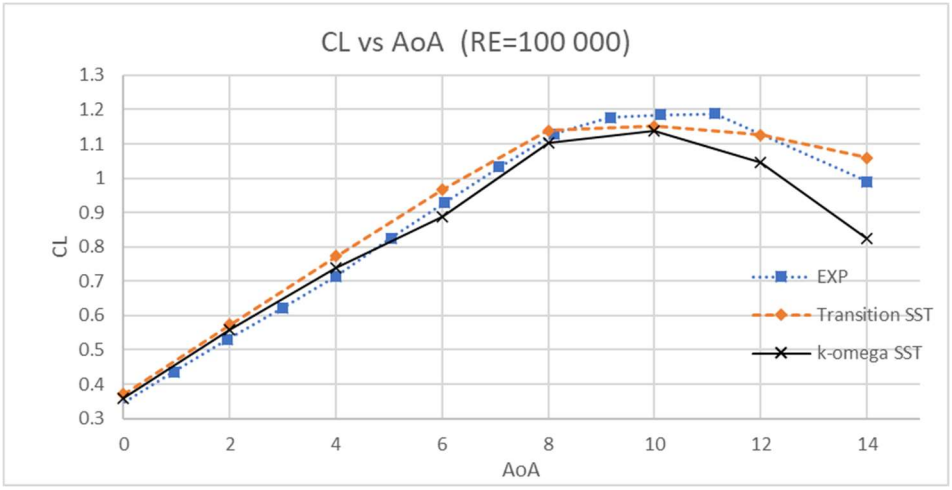

Figure 11, CL vs AoA at RE 100000 with Transition SST, k-omega SST, and the Experimental Data

As shown in Figure 12, the CD values of the k-omega SST model has given a similar trend in comparison to the experimental data where both sets of data have an initial peak before CD increases drastically however the k-omega model predicts this initial peak at AoA 6° whereas this peak is at AoA 4° for the experimental data. The Transition SST model has not captured this initial peak at all and the CD values deviate up to 37.6% both models could not produce CD values constant within 10% of the experimental data therefore further simulations of the E387 aerofoil with a GF will provide false CD values hence this simulation cannot be validated for the 100,000 Reynolds flow with both models.

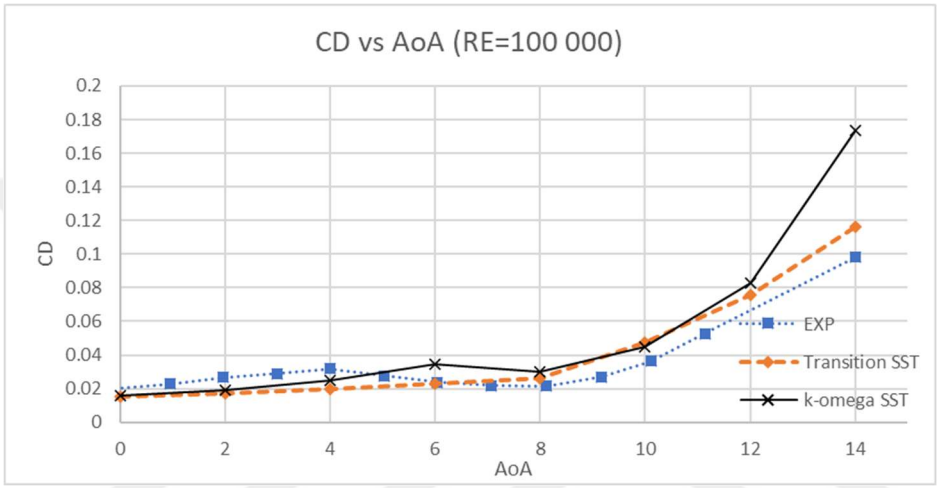

Figure 12,CD vs AoA at RE 100000 with Transition SST, k-omega SST, and the Experimental Data

As shown in figures 13-14, Reynolds Flow of 200000, both models have provided very similar CL and CD values all within 10% of the experimental data apart from at AoA 14 where k-omega SST model underestimates the CL and overestimates the CD by 7% and 36%.

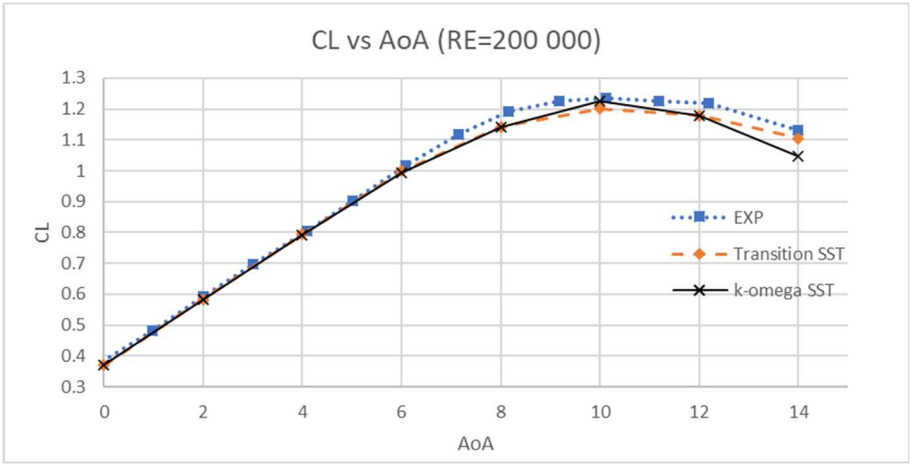

Figure 13,CD vs AoA at RE 200000 with Transition SST, k-omega SST, and the Experimental Data

Since both turbulence models show good correlation of the experimental data of A0A below 14°, the performance of the models must be tested to see the ability of both models to capture laminar separation bubble phenomena with the a GF attached to the aerofoil.

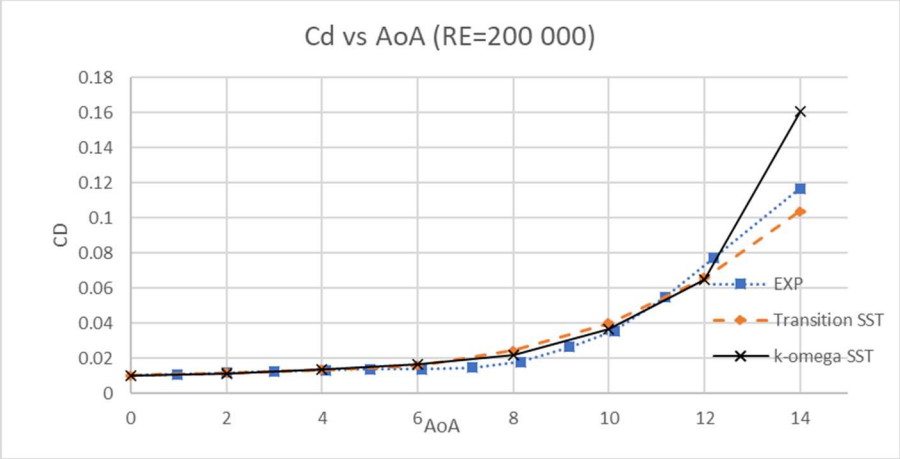

Figure 14,CD vs AoA at RE 200000 with Transition SST, k-omega SST, and the Experimental Data

4.2. Reynolds Effect on the Flow

The transition SST model is evaluated in the Figure 15 below showing the transition onset of the laminar separation bubble (LSB) that forms on the upper surface of the aerofoil. The transition onset point is observed when the coefficient of friction on the surface of the aerofoil is 0. Since the k-omega SST model has provided similar results it is not duplicated in this section but instead shown in Appendix A figures 31 and 32.

Since the adverse pressure gradient (APG) is the same at each AoA, it was expected that the transition onset would be very similar between the two Reynolds settings. Figure 15 shows that the LSB onset gradually moves toward the leading edge from the chord midpoint at AoA's 0° to 6°. At AoA 8° the LSB onset moves right to the leading edge of the aerofoil as the APG at AoA 8° is too high. Hence, the flow separates as a shear layer due to the low kinetic energy of the laminar boundary layer.

The main noticeable difference between the two Reynolds settings is the length of the LSB formed. Figure 16 and 17 shows the flow over the aerofoil at AoA 10° with Reynolds 100,000 and 200,000. The LSB formed in figure 16 is much longer than the LSB formed in Figure 17. This is because at lower Reynolds flow, once the flow separates as a shear layer, the momentum gained from the free stream is less than the momentum gained at higher Reynolds flow therefore it takes longer for the separated sheer layer to gain enough momentum from the free stream and reattach to the surface at low Reynolds flow. Resulting in the formation of longer LSB in comparison to the LSB formed at Higher Reynolds.

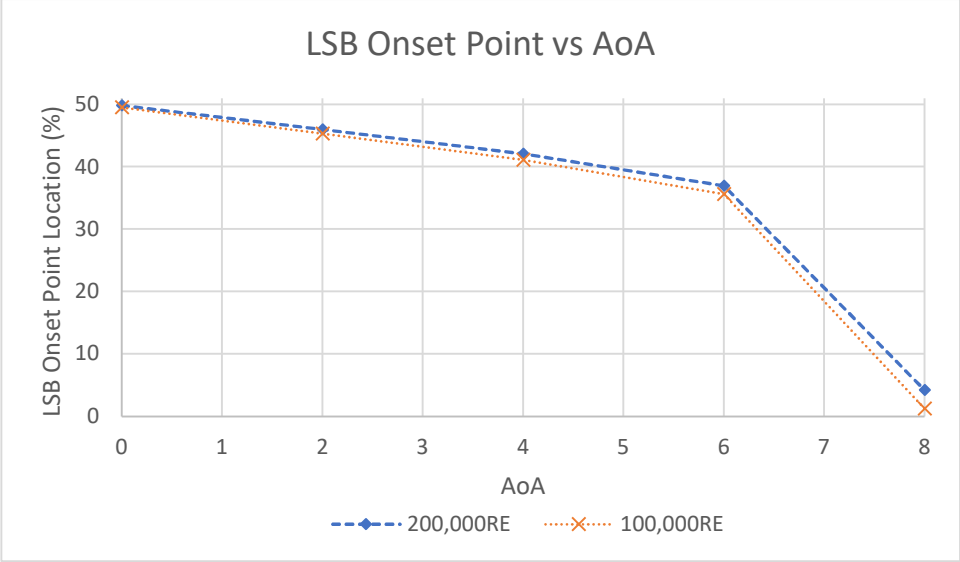

Figure 15, LSB Transition Onset vs AoA

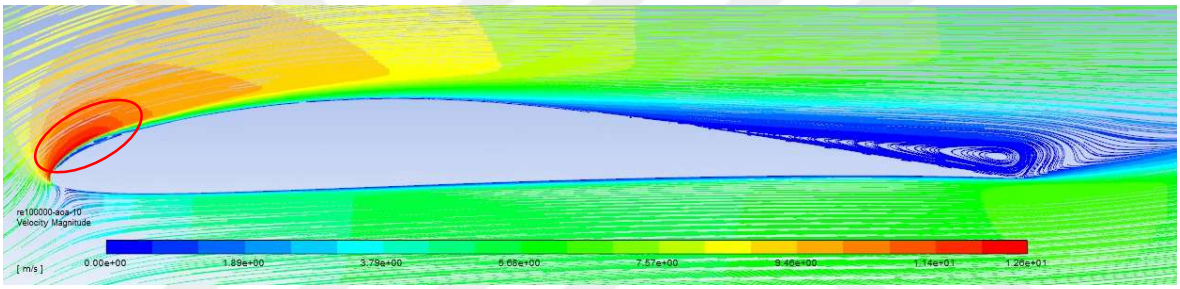

Figure 16, AoA 10, 100,000RE Velocity Profile

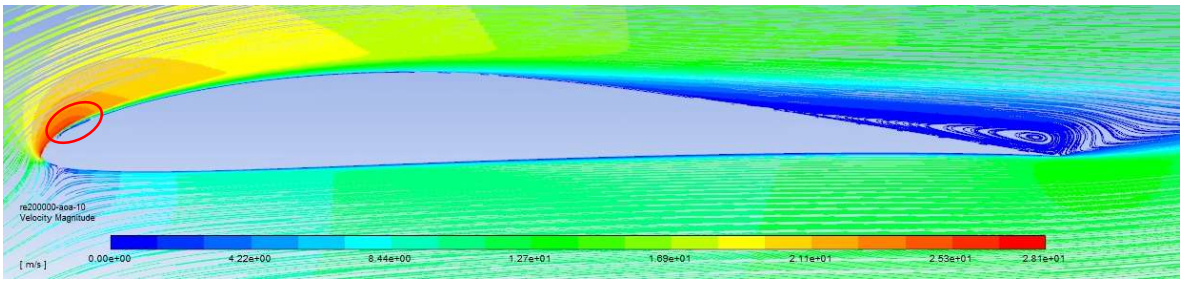

Figure 17, AoA 10, 200,000RE Velocity Profile

4.3. Choosing Turbulence Model

Since the transition SST and the k-omega SST models both provided results that were validated by the experimental data at 200,000 Reynolds flow. Both models were initially used to model the influence of the GF on the E387 aerofoil. It was quickly noticeable that both models were producing similar CL and CD values, but it was visible that the k-omega SST model could not capture the full formation of LSB of the aerofoil with the GF as shown in figure 18 which represents the velocity profile over the aerofoil at AoA 4° where no LSB was captured whereas it was captured by the transition SST model shown in Figure 19. The CL and CD across AoA with different GF heights are presented in appendix A by figures 33-34.

This correlates well with the research conducted by Aftab *et al.,* (2016) on the accuracy of turbulence models to capture the LSB phenomenon as it was stated that the K-omega SST model is unable to fully capture the LSB where as the transition SST model can predict the flow behaviour at low and high angles accurately.

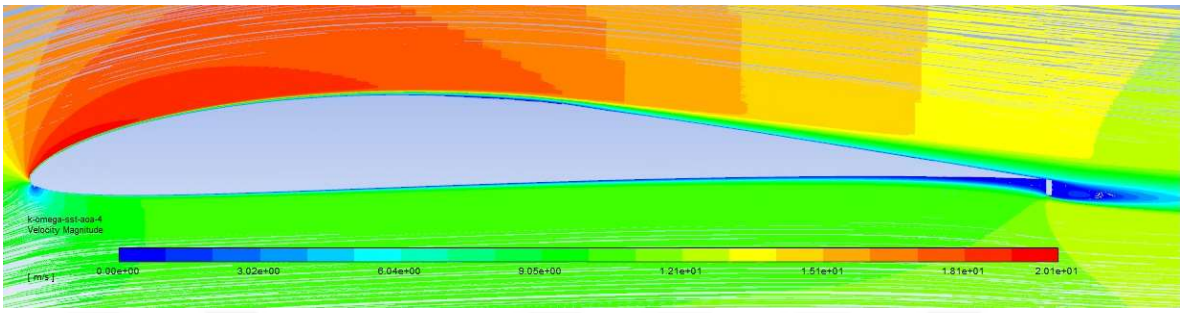

Figure 18, k-omega SST Model, AoA 4, 200,000RE

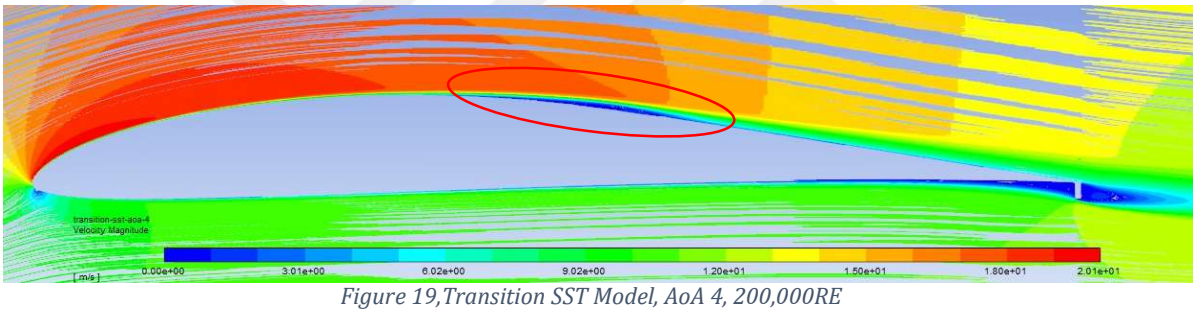

Figure 19,Transition SST Model, AoA 4, 200,000RE

The k-omega SST model was investigated to see if it would be suitable for the low Reynolds flow over the E387 aerofoil. What lead to this model being chosen is that the model predicted accurate CL, CD and LSB formation with no GF. If the model did provide expected flow behaviour with the GF, computational time and cost to simulate rest of the scenarios would be reduced in comparison to the use of the Transition SST model which is made up of four equations whereas K-omega SST model is made up of 2 equation. Hence, the transition SST model is used to simulate the low Reynolds flow over the E387 aerofoil prioritising accuracy of the flow characteristics.

4.4. Gurney Flap Influence on CL and CD

The effect of a GF on the E387 on the CL and CD is shown in Figures 20-21. It is evident that the CL increases as GF height increases. This is also applicable for the CD. At AoA 0° the CL is increased for GF heights of 1c%, 1.5c%, 2c% and 3c% by 34%, 56%, 78% and 107%. The corresponding drag coefficients increased by 1%, 21%, 47% and 88%. It is evident that the drag penalty above 2c% GF height would not be beneficial for efficiency as the drag penalty is too high resulting in lower lift to drag ratios that would not perform as well as a rotor.

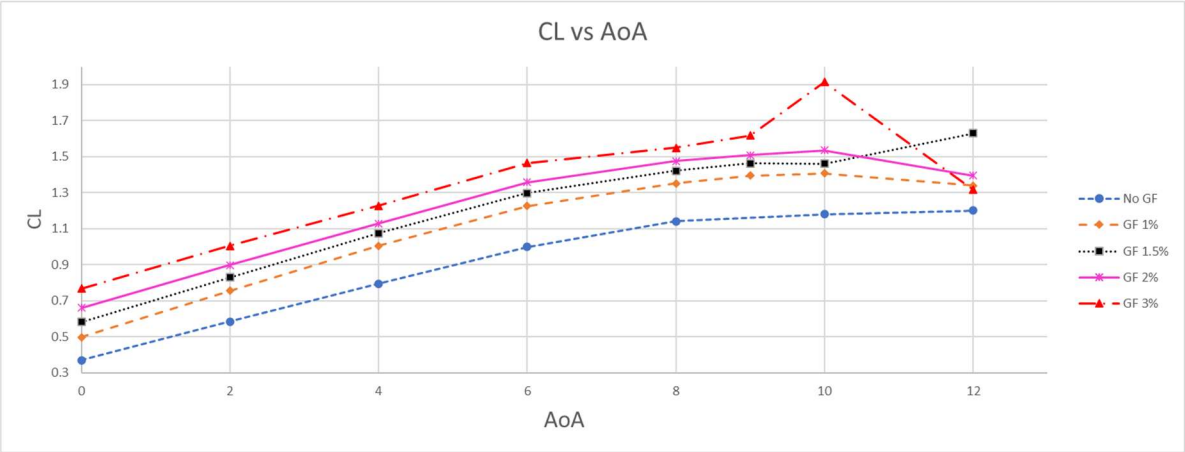

Figure 20, CL vs AoA All GF Settings

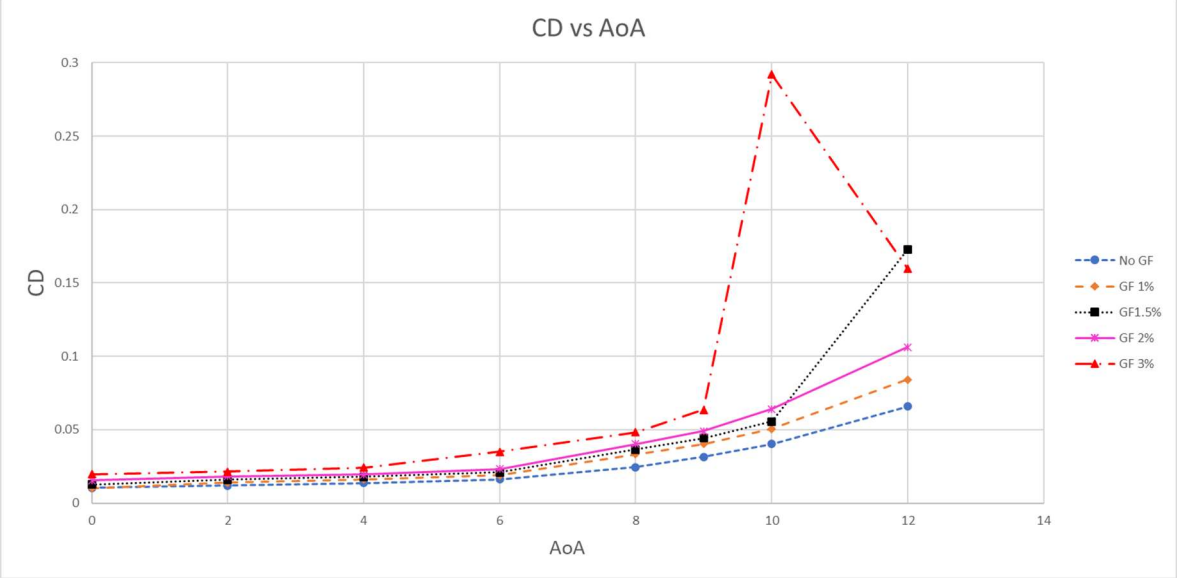

Figure 21, CD vs AoA All GF Settings

Figure 20-21 shows that the CL increases drastically at AoA 10 for GF height 3c%. This is because stall vortices are forming on the upper surface of the aerofoil shown in figure 22. The solution becomes unstable when stall vortices are forming hence full convergence of 1e-5 was not achieved for GF 3c% height at AoA 12° and 14°.

The early formation of stall with the highest GF height shows that the stall angle is reduced. Therefore, it can be said that the increase in lift coefficient comes at a cost of reduced stall angle which also correlates with the findings of Yan *et al.*, (2019) as their research also showed that the stall angle reduces with GF height.

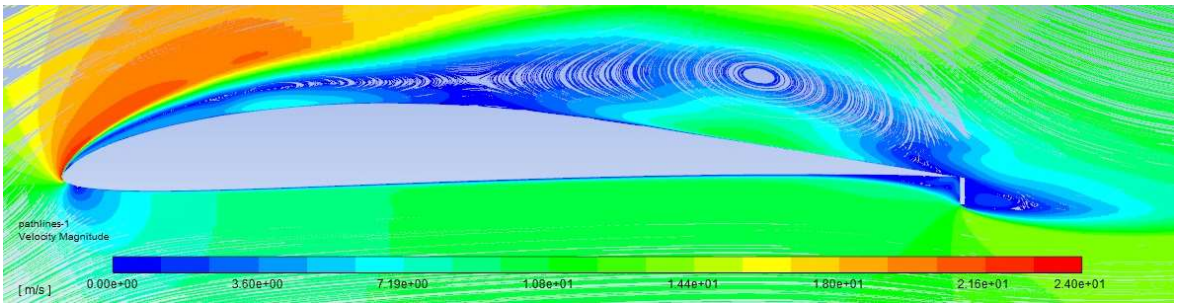

Figure 22, GF 3c% AoA 10 Stall Vortices

Figure 23 represents the CL/ CD ratio against the angle of attack. High CL/CD ratio is critical in improving the efficiency of a wind turbine blade. This graph shows the consequences of the drag penalty induced by the GF at high angles of attack and increasing GF height.

With a 1c% GF height, the CL/CD ratio at AoA 0° is increased by 36.2% which gradually reduced to an increase of 4.6% at AoA 6° in comparison to the aerofoil without GF. With 1.5c% GF height, the CL/CD ratio is initially increased by 28.9% but is then abruptly reduced to an increase of 0.2% by AoA 6°. It is plausible to say with increasing GF height the sooner the CL/CD ratio becomes lower than the CL/CD ratio of the aerofoil without GF as shown in figure 23.

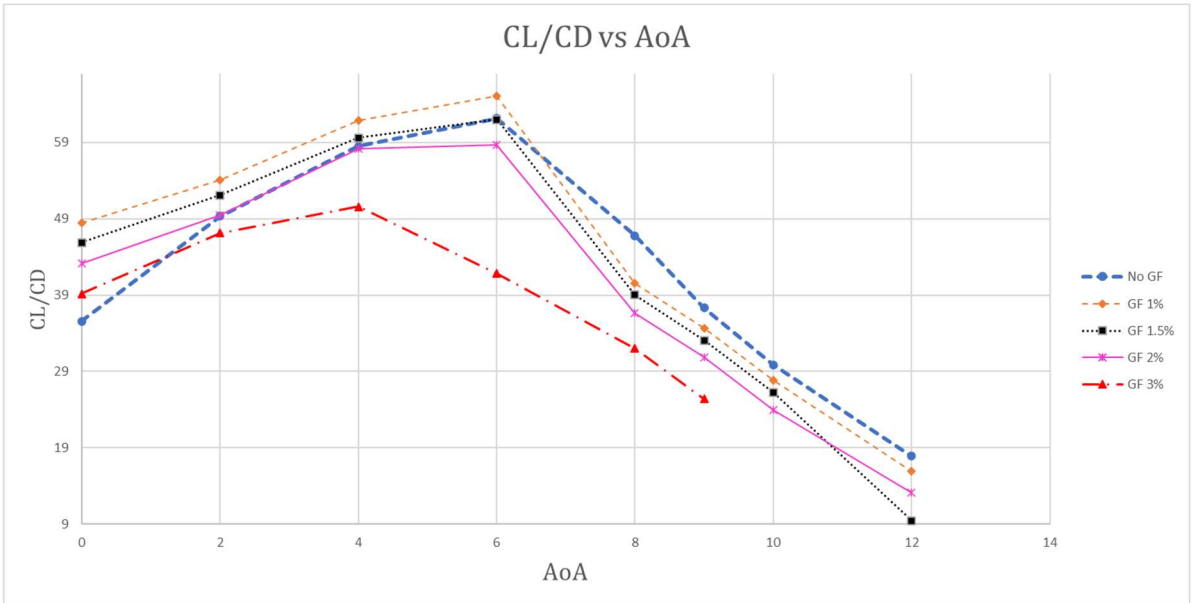

Figure 23, CL/CD against AoA

All GF heights apart from 3c% experience a drop CL/CD ratio after AoA 6° and show lower values for higher AoA's than the aerofoil without GF although, as shown in figure 20, the CL is consistently higher with a GF at all angles of attack. Hence it is fair to say that the GF drag penalty becomes much more severe at higher angles of attack especially after AoA 6° for all GF heights apart from the 3c% GF.

At 3c% GF height the CL/CD ratio starts declining earlier at AoA 4° and is showing lower values in comparison to the aerofoil without GF from approximately AoA 1°.

To be able to visualise how the change in pressure between the top surface and the bottom surface of the aerofoil is effected by a GF, the coefficient of pressure is also plotted against the length across the chord of the aerofoil as shown in Figure 23. It is visible that with the Gurney flap Size increasing the overall pressure difference between the two surfaces also increase, especially near the trailing edge. Yan *et al.*, (2019) discovered that the loading does not improve of GF height larger than 2c%. In this case we can see that the change in CP does increase at 3c%. This difference in results could be because Yan *et al.*, has performed the investigation on a symmetrical aerofoil at 160,000 Reynolds whereas the E387 is an asymmetrical aerofoil and performed at 200,000 Reynolds.

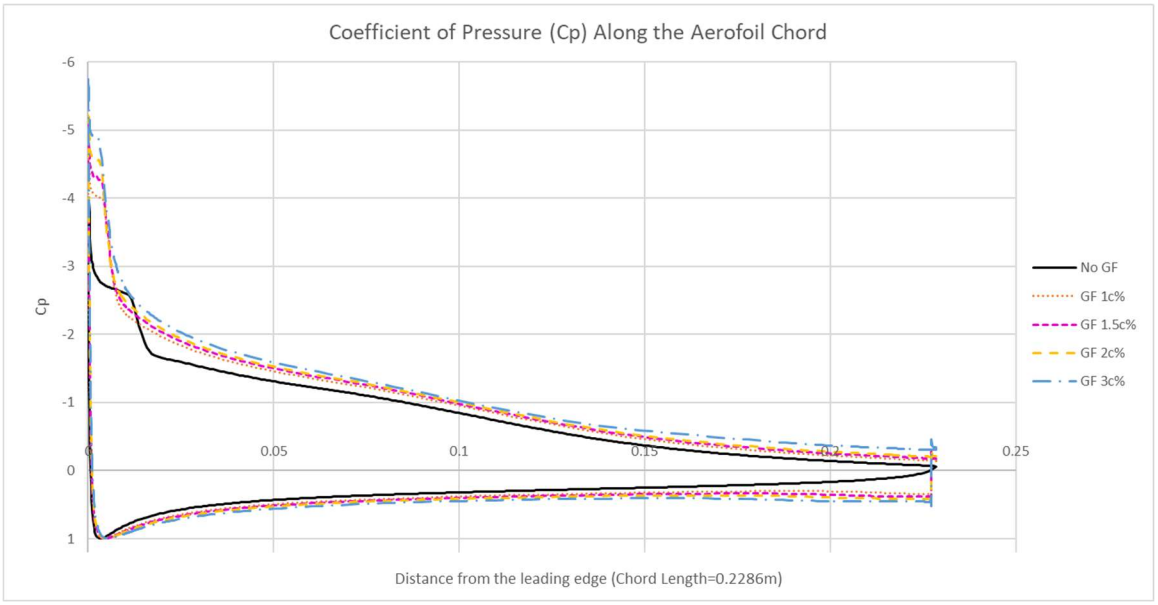

Figure 24, Coefficient of pressure across the chord of the aerofoil at AoA 9

It is also visible that the aerofoil without GF has initial steep increase of Cp on the upper surface of the aerofoil later and for a longer distance across the aerofoil where this is experienced sooner and shorter for all of the GF heights. This characteristic of the Cp graph represents the formation of an LSB. This sudden change in Cp means that the LSB formed with the GF develops a shorter LSB sooner than the aerofoil without GF. This was then confirmed in figures 25 and 26 where the flow diagrams are shown.

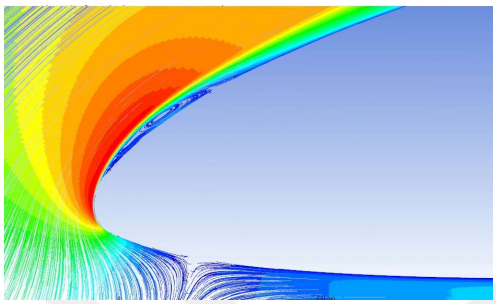

Figure 25, LSB with GF at AoA 9

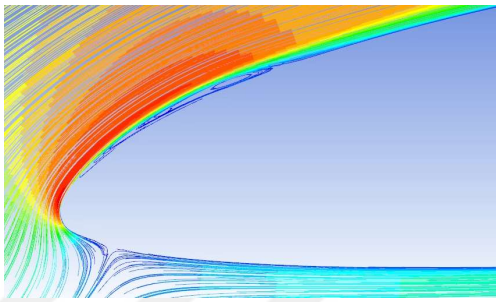

Figure 26, LSB without GF at AoA 9

4.5. Control of LSB by the Trailing Edge

Figure 27 represents the E387 aerofoil trailing edge at AoA 0° where the flow is smooth and there are no separation regions. Figure 28 shows the effect of a GF with 1.5c% height where a stagnation zone upstream of the GF and two counter rotating vortices downstream of the GF are formed. This is also evident in the research produced by Leibeck (1978) and the numerical analysis performed by Yan *et al.*, (2019).

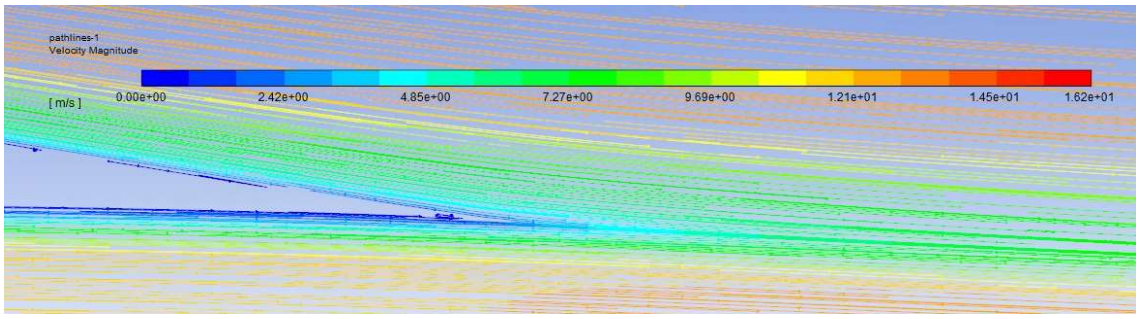

Figure 27, AoA 0, 200,000RE Trailing Edge

It can be seen in figure 28 that the vortices formed by the GF causes a downward turning of the flow at the trailing edge. It is visible in figures 27 and 28 that the flow velocity is higher on the suction side of the aerofoil with the GF. This is caused by the downward momentum of the flow which increases with increasing GF height. This is a key feature that is observed at low AoA and

with increasing AoA the GF acts in a way to delay the formation of separation near the trailing edge which can utilise the effective chord length of the aerofoil and is discussed below.

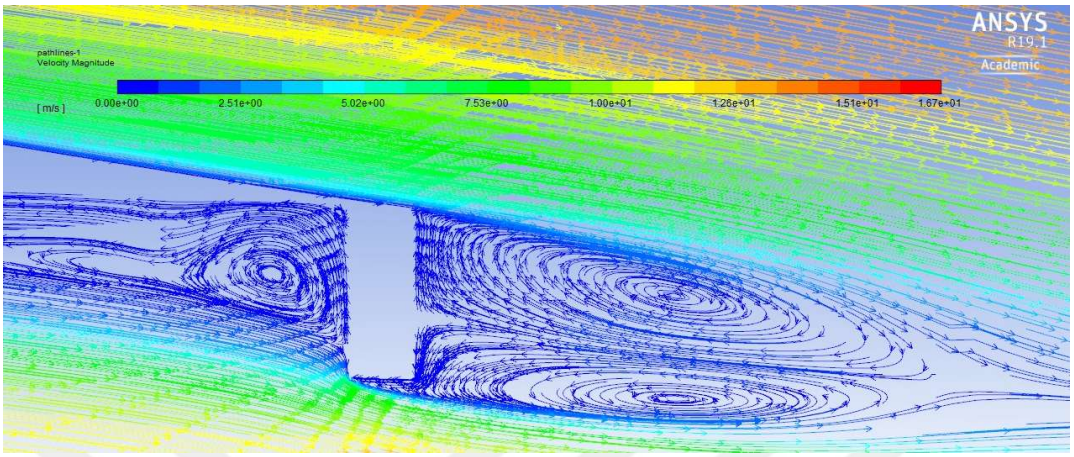

Figure 28, AoA 0 GF 1.5c% Trailing Edge

It is observed that at an AoA 9° in Figure 30, that two separation regions form on the downstream and upstream of the GF. These two counter rotating vortices reduce adverse pressure gradient which is effective at the trailing edge of the aerofoil. This causes the delay of the separation region which is evident in Figure 29 where the trailing edge separation forms, but it is suppressed in figure 30. Therefore, the effective chord length is increased resulting in increase of lift.

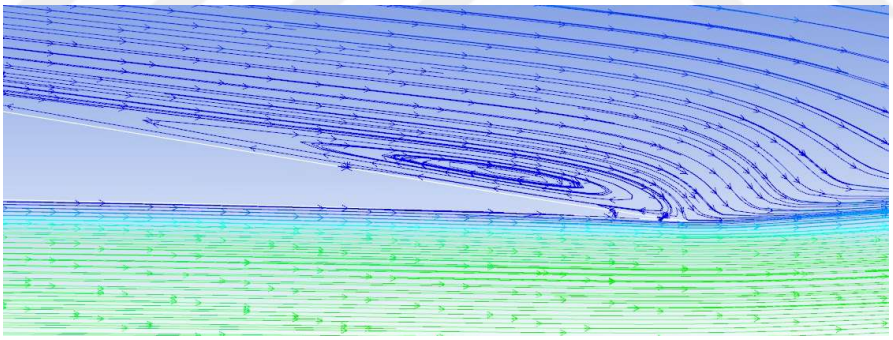

Figure 29, AoA 9 No GF Trailing Edge

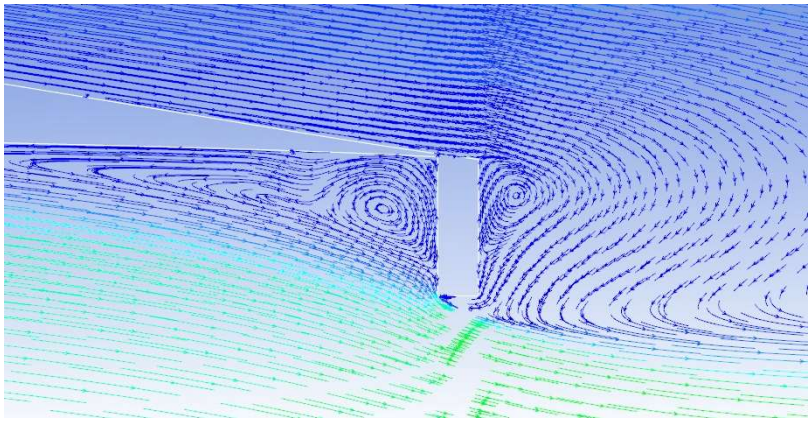

Figure 30, AoA 9 1.5c% GF Trailing Edge

4.6. Coefficient of Power (CP) of a Single Rotor Assuming Linear Aerodynamics

Table 3 shown below shows all the variables calculated and used to find the optimum coefficient of power (CP_{opt}). It is seen that with increasing Cl_{opt}, the TSR_{opt} reduces. GF heights 1c% and 3c% reduced the CP_{opt} in comparison to the aerofoil without GF. GF height of 1.5c% did not change the CP_{opt} however it is achieved at a lower TSR_{opt}. The 2c% GF height experienced a reduction of 14.1% TSR_{opt} and an increase of 12% of CP_{opt}. Hence, for operating conditions of 3.0 to 3.5 TSR, the GF height of 2c% provides the highest improvement of the coefficient of power.

This adheres well with Liebeck (1978) research as it was also found that the GF height should be kept between 1% and 2% chord length of the airfoil to maximize the aerodynamic benefits which otherwise could be invalidated by the increase in drag

Table 3, Calculation of the Coefficient of Power

	Cl_{opt}	CD	$Cl\alpha$	TSR_{opt}	Flow Angle	Pitch Angle	CP_{opt}
No GF	1	0.0161	6.00	3.563	0.187	-0.146	0.451
GF 1c%	1.226	0.0188	6.96	3.219	0.207	-0.145	0.404
GF 1.5c%	1.298	0.0209	6.84	3.128	0.213	-0.166	0.451
GF 2c%	1.357	0.0231	6.65	3.059	0.218	-0.190	0.506
GF 3c%	1.228	0.0243	6.64	3.216	0.207	-0.162	0.450

5. Conclusion:

Overall, all objectives were completed to achieve the aim of investigating and optimizing the effect of a Gurney Flap on Eppler E387 low Reynolds number profile airfoil and its effect on a small-scale Horizontal Axis Wind Turbine (HAWT) performance.

Literature review and study of methodology was successfully performed to gain knowledge of existing research and the feasibility of this project. High level of CFD ANSYS software skills were developed to model the laminar separation bubble phenomena.

2D CFD analysis of the E387 aerofoil without gurney flaps at low Reynolds of 100,000 and 200,000 was carried out to validate the numerical analysis so that further simulations with gurney flaps could be performed accurately. This led to the discovery that the 200,000 Reynolds flow simulation would provide results with higher accuracy. Overall, the results from this validation showed that the numerical results matched well with the experimental results obtained from literature. It was seen that the K-omega SST model failed to capture the laminar separation bubble phenomena with the inclusion of the gurney flap when compared to the four equation Transition SST model.

2D CFD analysis of the E387 profile aerofoil with four different Gurney Flap heights of 1c%, 1.5c%, 2c% and 3c% were investigated. The airflow characteristics around the aerofoil caused by the gurney flap obtained from the simulations matched with the current research where the lift was enhanced with increasing Gurney Flap height due to the distinctive counter rotating vortices formed by the gurney flap. However, at high AoA the drag penalties became more severe which leads to an earlier stall. This investigation has also shown that that flow separation near the trailing edge of the aerofoil is supressed and that the aerofoil loading is drastically improved with the increase of GF height.

The optimum CL/CD ratios of each Gurney Flap setting was used to calculate the optimum tip speed ratio and the coefficient of power. This led to the discovery that the 2c% GF height is the optimum height considering the rotor conditions between 3 to 3.5 TSR with an improvement of optimum coefficient of power of 12% in comparison to the aerofoil without GF.

5.1. Future Work

Future work can be implemented on this investigation by calculating the thrust generated by the rotor to see the effect of the GF in higher detail. Furthermore a detailed Blade Element Method can be used to estimate the annual energy production of the wind turbine to contribute to designing small scale wind turbines that are highly effective, with low Reynolds flow, with the E387 aerofoil and Gurney Flap.

6. References:

- Aftab, S., Mohd Rafie, A., Razak, N. and Ahmad, K., 2016. Turbulence Model Selection for Low Reynolds Number Flows. *PLOS ONE*, 11(4), p.e0153755.
- ANSYS Inc. (2009). *4.1 Introduction*. Retrieved from ANSYS Fluent Theory Guide 12.0: https://www.afs.enea.it/project/neptunius/docs/fluent/html/th/node43.htm
- Aramendia, I., Fernandez-Gamiz, U., Zulueta, E., Saenz-Aguirre, A. and Teso-Fz-Betoño, D. (2019). Parametric Study of a Gurney Flap Implementation in a DU91W(2)250 Airfoil. Energies, 12(2), p.294.
- Avital, E., 2020. *C_P_Opt_Procedure,* Private Communication.
- Bianchini, A., Balduzzi, F., Di Rosa, D. and Ferrara, G., 2019. On the use of Gurney Flaps for the aerodynamic performance augmentation of Darrieus wind turbines. *Energy Conversion and Management*, 184, pp.402-415.
- Chen, L., Xie, H., Xu, J., Dai, R. and Chen, J. (2018). Experimental and numerical study on the performance of an axial fan with a Gurney flap. Advances in Mechanical Engineering, 10(10), pp. 1-17.
- Dilimulati, A., Stathopoulos, T. and Paraschivoiu, M. (2018). Wind turbine designs for urban applications: A case study of shrouded diffuser casing for turbines. Journal of Wind Engineering and Industrial Aerodynamics, 175, pp.179-192.
- Hansen, M., 2008. *Aerodynamics of Wind Turbines*. London: Earthscan.
- Hao, L. and Gao, Y., 2019. Effect of Gurney Flap Geometry on a S809 Airfoil. *International Journal of Aerospace Engineering*, 2019, pp.1-8.
- He, X., Wang, J., Yang, M., Ma, D., Yan, C. and Liu, P., 2017. Numerical simulation of gurney flaps lift-enhancement on a low Reynolds number airfoil. *Science China Technological Sciences*, 60(10), pp.1548-1559.
- Jang, C., Ross, J. and Cummings, R., 1998. Numerical investigation of an airfoil with a Gurney flap. *Aircraft Design*, 1(2), pp.75-88.
- Ledo, L., Kosasih, P. and Cooper, P., 2011. Roof mounting site analysis for micro-wind turbines. *Renewable Energy*, 36(5), pp.1379-1391.
- Liebeck, R., 1978. Design of Subsonic Airfoils for High Lift. *Journal of Aircraft*, 15(9), pp.547-561.
- Mayer, C., Bechly, M., Hampsey, M. and Wood, D., 2001. The starting behaviour of a small horizontal-axis wind turbine. *Renewable Energy*, 22(1-3), pp.411-417.

- Menter, F., Langtry, R. and Völker, S., 2006. Transition Modelling for General Purpose CFD Codes. *Flow, Turbulence and Combustion*, 77(1-4), pp.277-303.
- Ozgener, O. and Ozgener, L., 2007. Exergy and reliability analysis of wind turbine systems: A case study. *Renewable and Sustainable Energy Reviews*, 11(8), pp.1811-1826.
- Shen, X., Avital, E., Paul, G., Rezaienia, M., Wen, P. and Korakianitis, T., 2016. Experimental study of surface curvature effects on aerodynamic performance of a low Reynolds number airfoil for use in small wind turbines. *Journal of Renewable and Sustainable Energy*, 8(5), p.053303.
- Singh, R. and Ahmed, M., 2013. Blade design and performance testing of a small wind turbine rotor for low wind speed applications. *Renewable Energy*, 50, pp.812-819.
- Sreejith, B. and Sathyabhama, A., 2018. Numerical study on effect of boundary layer trips on aerodynamic performance of E216 airfoil. *Engineering Science and Technology, an International Journal*, 21(1), pp.77-88.
- Tummala, A., Velamati, R., Sinha, D., Indraja, V. and Krishna, V., 2016. A review on small scale wind turbines. *Renewable and Sustainable Energy Reviews*, 56, pp.1351-1371.
- Winslow, J., Otsuka, H., Govindarajan, B. and Chopra, I., 2018. Basic Understanding of Airfoil Characteristics at Low Reynolds Numbers (104–105). *Journal of Aircraft*, 55(3), pp.1050-1061.
- Xiang, S., 2017. *Experimental and Numerical Study Of Surface Curvature Effects On The Performance Of The Aerofoils Used In Small Wind Turbines*. PhD. Queen Mary University of London.
- Yan, Y., Avital, E., Williams, J. and Cui, J., 2019. Performance Improvements for a Vertical Axis Wind Turbine by Means of Gurney Flap. *Journal of Fluids Engineering*, 142(2).

Appendix A:

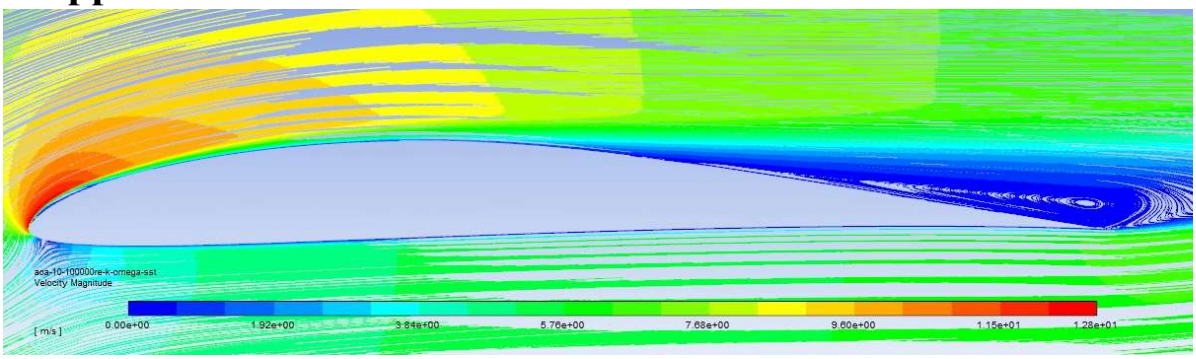

Figure 31, AoA 10, 100000 RE flow with the k-omega SST model

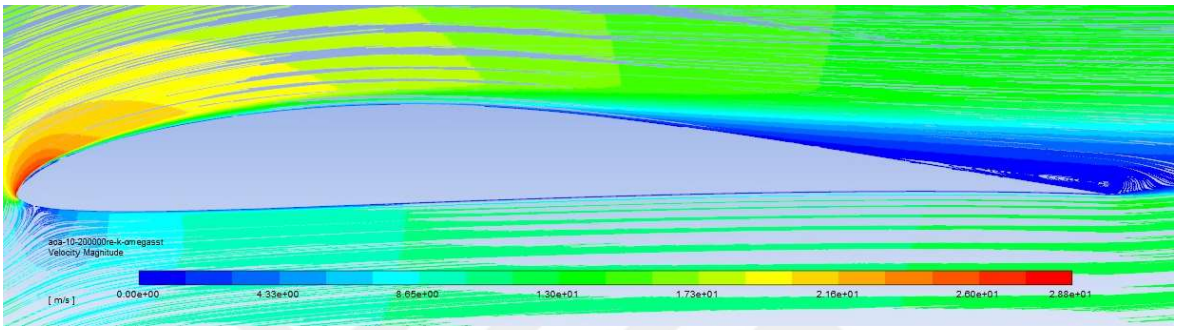

Figure 32, AoA 10, 200000 RE flow with the k-omega SST model

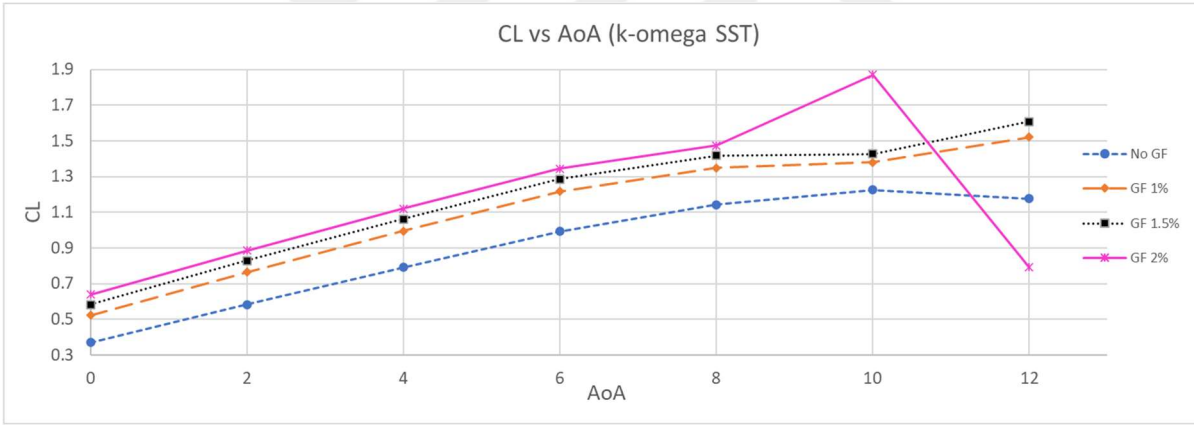

Figure 33, CL against AoA of GF configuration with the K-omega SST model

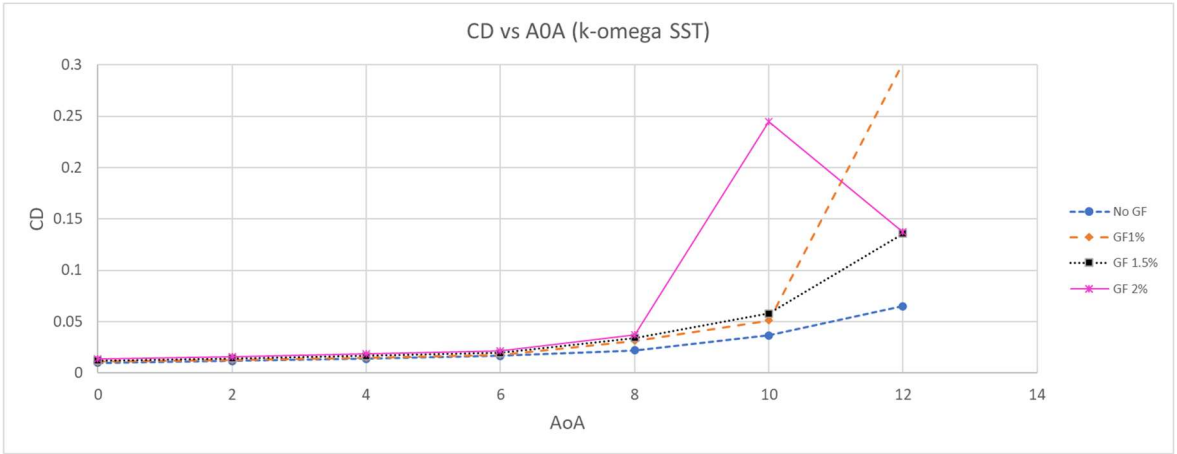

Figure 34, CD against AoA of GF configuration with the K-omega SST model

Appendix B

BEM High TSR, neglecting drag

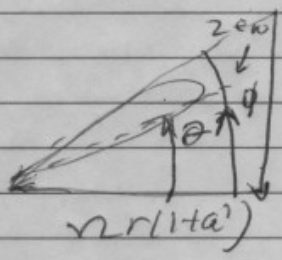

$$\tan\phi = \frac{1-a}{TSR \cdot x(1+a')} \qquad x = r/R \qquad (1)$$

$$\frac{a}{1-a} = \frac{\sigma C_L \cos\phi}{4\sin^2\phi} \qquad \text{axial momentum} \qquad (2)$$

$$\frac{a'}{1-a'} = \frac{\sigma C_L}{4\cos\phi} \qquad \text{Torque} \qquad (3)$$

$$\alpha = \phi - \theta \Rightarrow C_L = C_{L_\alpha} \cdot \alpha$$

Assuming $\phi << 1\,rad$, $a' << 1$, $TSR >> 1$

$\hookrightarrow \phi \simeq \sin\phi \simeq \tan\phi$

$1+a' \simeq 1$

From (2) we get

$$\frac{a}{1-a} = \frac{\sigma C_L}{4\phi^2}$$

$$\hookrightarrow \sigma C_L \alpha = \frac{4a\phi^3}{1-a} = \frac{4}{TSR^3 x^3}\,a(1-a)^2$$

From optimal BEM $a = 1/3$

$$\hookrightarrow \sigma C_{L_{opt}} = \frac{8}{9\,TSR^2 \cdot x^2}$$

$$\hookrightarrow \boxed{TSR^2_{opt} = \frac{8}{9\sigma C_{L_{opt}}}} \quad \text{assuming } C_{L_{opt}} \qquad (4)$$

at the tip $x=1$.

After finding TSR_{opt} from (5), find

$$\Phi_{opt} = \frac{2}{3 \cdot TSR_{opt}} \quad (5)$$

$$\theta_T = \frac{2}{3 \cdot TSR_{opt}} \left(1 - \frac{8}{3 TSR_{opt} C_{l_d} \sigma}\right) \quad (6)$$

And

$$C_{P_{opt}} = \frac{TSR^3_{opt} \sigma C_{l_d} \theta_T (\Phi_T - \theta_T)}{2} \quad (7)$$

$$- \frac{\sigma C_{D_0} TSR^3}{2}$$

Where C_{D_0} is the C_D at optimal C_L

In this analysis, the blade with GT is twisted differently than the blade with no GF.

calculation procedure:

1. Take $\sigma = 0.1$,
2. $C_{L_{opt}}$ is the C_L you want the blade to operate. Find the C_D as C_{D_0} from CFD.
3. Find TSR_{opt} from Eq(4)
4. Find θ_T and Φ_T from Eqs (6) & (5)
5. Find $C_{P\,opt}$ from Equ (7)

– 2 –

Figure 35, Private Communication with Dr Avital